GSDeformer: Direct, Real-time and Extensible Cage-based Deformation for 3D Gaussian Splatting

Jiajun Huang*, Shuolin Xu*, Hongchuan Yu*, Tong-Yee Lee†
*National Centre for Computer Animation, Bournemouth University
†Department of Computer Science and Information Engineering, National Cheng-Kung University

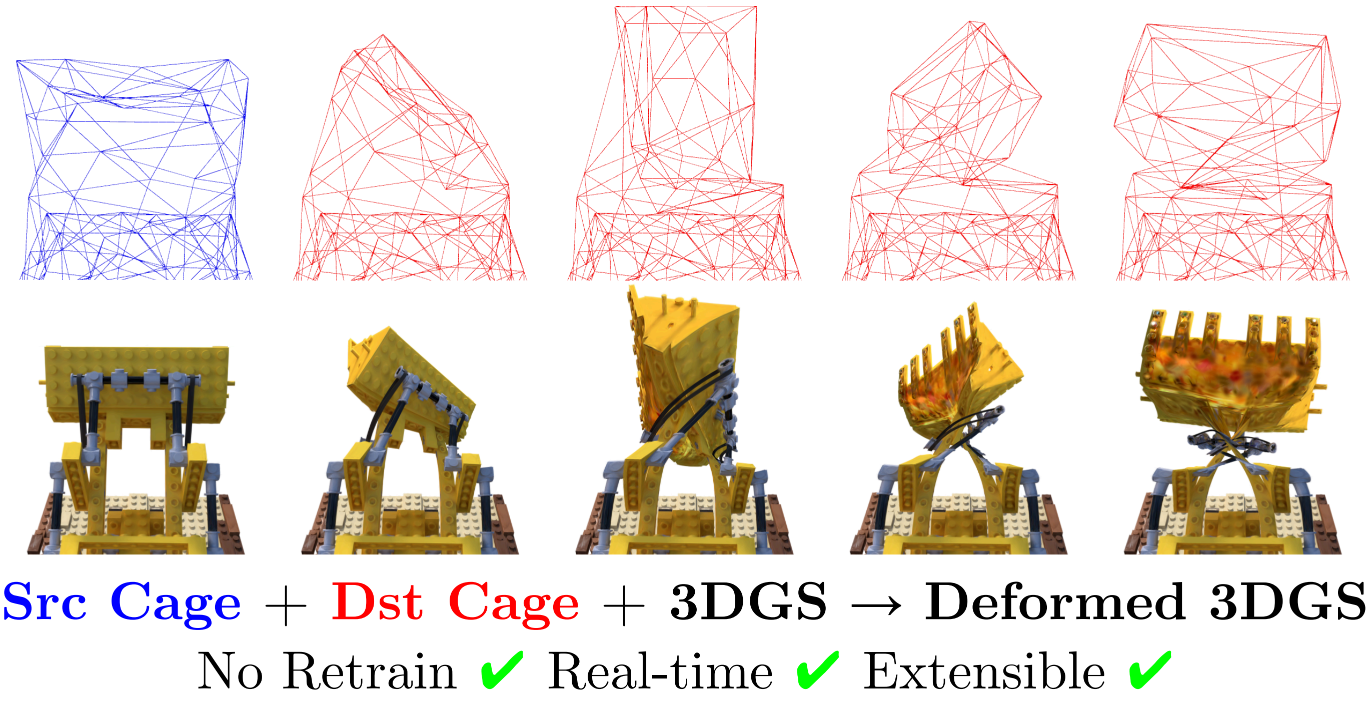
Src Cage + Dst Cage + 3DGS → Deformed 3DGS
No Retrain ✔ Real-time ✔ Extensible ✔

***Abstract*—We present GSDeformer, a method that enables cage-based deformation on 3D Gaussian Splatting (3DGS). Our approach bridges cage-based deformation and 3DGS by using a proxy point-cloud representation. This point cloud is generated from 3D Gaussians, and deformations applied to the point cloud are translated into transformations on the 3D Gaussians. To handle potential bending caused by deformation, we incorporate a splitting process to approximate it. Our method does not modify or extend the core architecture of 3D Gaussian Splatting, making it compatible with any trained vanilla 3DGS or its variants. Additionally, we automate cage construction for 3DGS and its variants using a render-and-reconstruct approach. Experiments demonstrate that GSDeformer delivers superior deformation results compared to existing methods, is robust under extreme deformations, requires no retraining for editing, runs in real-time, and can be extended to other 3DGS variants. Project Page: https://jhuangbu.github.io/gsdeformer/**

***Index Terms*—3D Gaussian Splatting, Cage-based Deformation, 3D Representation Editing, Animation**

I. Introduction

3D Gaussian Splatting (3DGS) [1] is a novel and efficient approach for reconstructing and representing 3D scenes. Due to its ability to capture real-world objects and environments in impressive quality, it holds significant potential for downstream applications such as animation, virtual reality, and augmented reality. To make 3DGS practical for these applications, it is crucial to enable users to freely edit the captured scenes for privacy or creative purposes.

Current methods do not achieve direct, real-time, and extensible manipulation of 3D Gaussian Splatting (3DGS). Techniques like DeformingNeRF [2], CageNeRF [3], and NeRF-Shop [4], which enable cage-based deformation on Neural Radiance Fields (NeRF), work by deforming sample points during the volumetric rendering process. However, since 3DGS does not use volumetric rendering, these methods cannot be easily adapted to it, restricting them to the more expensive-to-train and lower-quality NeRF-based representations.

Existing methods for editable 3DGS, such as GaMeS [5], Gaussian Frosting [6], and SC-GS [7], require significant modifications to the 3DGS representation or impose additional requirements on the training data, leading to the need for retraining. This limitation prevents these methods from directly editing existing 3DGS captures without extensive retraining, also making them harder to integrate with other 3DGS-derived scene representations. Methods like SC-GS [7] and VR-GS

[8] that allow manual editing rely on control structures such as tetrahedral grids or control point clouds, which are less convenient for integration with existing animation software and pipelines.

To address these challenges, we propose GSDeformer, a method that enables cage-based deformation on trained vanilla 3DGS models and their variants. Our approach operates directly on trained 3DGS without requiring extensive retraining, performs deformation in real time, and can be easily extended and integrated with other methods that enhance or build upon 3DGS.

Our approach leverages Cage-Based Deformation (CBD), which uses a coarse mesh (cage) to control deformations of the finer geometry within it. To deform the Gaussian distributions that make up the 3DGS representation, we generate a proxy point cloud from the Gaussians and apply CBD to deform the point cloud. The deformed proxy points then drive the transformations applied to the Gaussians. To handle potential bending caused by deformation, we introduce a splitting process for the relevant Gaussians.

This direct deformation approach enables editing of any trained vanilla 3DGS model without requiring architectural modifications or retraining. It also ensures compatibility with other 3DGS variants. Additionally, by using standard triangular cage meshes to control deformation, our method seamlessly integrates with existing animation software and pipelines.

Cages for deformation can be created either manually or automatically from 3DGS using our automated algorithm. Our automatic cage-building algorithm supports not only 3DGS but also its variants, such as 2DGS [9], through a render-reconstruct-simplify approach.

We evaluate the effectiveness of our method on object datasets. The results demonstrate that our deformation algorithm delivers superior quality compared to existing methods, particularly under extreme deformations. Among methods that enable explicit control, our control structure is the easiest to integrate with existing software. Furthermore, our algorithm achieves real-time performance ($\sim 60FPS$), renders deformed representations at high speeds ($> 200FPS$), and can be extended to other 3DGS variants.

In summary, our contributions include:

- We propose GSDeformer, a method achieving real-time cage-based deformation on any trained 3D Gaussian Splatting(3DGS) model without re-training or altering its core architecture.
- We also propose a robust automatic cage-generation algorithm that works on 3DGS as well as its variants due to its render-reconstruct-simplify approach.
- We conduct extensive experiments to demonstrate our method's ease of integration with other work extending 3DGS, as well as showing our method's superior quality and ease-of-control against existing methods under normal and extreme scenarios.

II. Related Work

A. Editing 3D Gaussian Splatting Scenes

Many methods have been proposed to edit 3D Gaussian Splatting (3DGS) models. There are high-level, textual-prompt-based editing methods such as GaussianEditor [10], VcEdit [11], and GaussCtrl [12], as well as other lower-level, more explicit editing methods.

To enable low-level, explicit editing, one effective approach is binding the Gaussian distributions in 3DGS to a mesh surface. Deforming 3DGS is then achieved by deforming the proxy mesh. SuGaR [13] pioneered this approach by proposing an algorithm that extracts mesh from 3DGS, along with training regularizations to improve the quality of the extracted mesh. GaussianFrosting [6] builds on it by proposing a more flexible way to bind distributions to the mesh. Both GaMeS [5] and Gao et al. [14] start with a provided initial mesh and train their models from there. While Mani-GS [15] does not need an initial mesh, it first trains a 3DGS or NeuS [16] model to create one, then uses this mesh as a base of its mesh-bounded Gaussian model.

While mesh-bounding methods can be effective, they have a significant drawback: they modify the core 3DGS architecture to handle deformation, requiring costly retraining, and even the initial mesh provided to them. This limitation makes it challenging to use these methods ([5], [6], [13]–[15]) for modifying existing trained 3DGS scenes or extending them to new variants of the standard 3DGS.

In contrast, our method directly operates on the Gaussian primitives in vanilla 3DGS representations, eliminating the need for retraining or extra data. This direct approach also makes it straightforward to adapt to different 3DGS variants, avoiding the complexity of integrating mesh-based architecture with these variants.

Many work have also explored physics-based simulation to manipulate 3DGS. PhysGaussian [17] uses the Material Point Method (MPM) [18] to model object deformation from touch and push interactions on 3DGS. Gaussian Splashing [19] integrates position-based dynamics (PBD) [20] with 3DGS for simulations. VR-GS [8] proposes a deformation approach similar to ours but relies on tetrahedral mesh grids with a large number of vertices. While this approach is designed for simulation, it is less suited for direct manual manipulation, which is the focus of our method. While these methods prioritize replicating natural physics, our approach emphasizes direct, user-controlled deformation and manipulation.

Previous work has also explored direct and manual manipulation of vanilla 3DGS models. SC-GS [7] enables Gaussian deformation by mapping control point transformations to Gaussians, but it requires video data for learning these mappings, limiting its applicability. Additionally, its control point-based formulation makes it challenging to adjust the scale of Gaussians. D3GA [21] achieves cage-based deformation on 3DGS but relies on tetrahedral mesh cages and is limited to 3DGS human bodies and garments. In contrast, our method uses standard triangular meshes, which are easier to edit, works on arbitrary 3DGS objects, and can be extended to variants of 3DGS.

Recent work ARAP-GS [22] proposes a 3D Gaussian deformation method that adapts the As-Rigid-As-Possible deformation approach and resolves spike-like artifacts by aligning deformed Gaussians with their corresponding radiance fields. However, this method is ineffective in handling extreme deformations, such as the Gaussian highlighted in Figure 14, which shows the bending of a single Gaussian. Our observation is that splitting bent Gaussian ellipsoids into multiple smaller ones is essential.

B. Cage-based Deformation

Cage-based deformation (CBD) is a family of methods that use a coarse mesh, called a cage, to control the deformation of a more detailed inner mesh.

CBD relies on cage coordinates to define how the positions of points within a cage relate to the cage's vertices, which are then used to define the deformation field. Various coordinate types, such as mean value coordinates (MVC) [23] [24], harmonic coordinates (HC) [25] [26], and green coordinates (GC) [27], have been developed, all demonstrating strong performance in mesh deformation.

Several methods, including DeformingNeRF [2], CageNeRF [3], NeRFShop [4], Li et al. [28], and VolTeMorph [29], have adapted cage-based deformation for radiance fields. These approaches deform sample points along rays during volumetric rendering. However, this strategy is incompatible with 3DGS, which uses rasterization instead of ray-based rendering. Our method addresses this challenge by adapting cage-based deformation to work with the Gaussian distributions that form the 3DGS representation.

For automatic cage construction, NeRFShop [4] employs marching cubes on the underlying opacity field to create a fine mesh, which is then simplified into a cage mesh using edge collapse [30]. Similarly, DeformingNeRF [2] begins with marching cubes but simplifies the mesh using Xian et al.'s method [31] instead of edge collapse.

In contrast, our novel cage-generation algorithm adopts a render-reconstruct-simplify approach. By combining T-SDF integration, depth carving, and simplification based on Bounding Proxy [32], our method can construct high-quality cages not only for 3DGS models but also for surface-like 3DGS variants (e.g., 2DGS [9]). Existing marching cube-based methods fail on these variants because they cannot be easily converted into opacity fields.

III. Method

A. Preliminaries

3D Gaussian Splatting 3D Gaussian Splatting (3DGS) [1] is a method for representing 3D scenes using a set of 3D Gaussians. Each Gaussian is characterized by its mean $\mu \in \mathbb{R}^3$, covariance $\mathbf{\Sigma} \in \mathbb{M}^{3x3}$, opacity $\alpha \in \mathbb{R}$, and color parameters $\mathcal{P} \in \mathbb{R}^k$. The color is view-dependent, modeled using spherical harmonics with k degrees of freedom. The covariance $\mathbf{\Sigma}$ is decomposed as $\mathbf{RSSR}^\mathsf{T}$, where $\mathbf{R}$ is a rotation matrix (encoded as a quaternion) and $\mathbf{S}$ is a scaling matrix (encoded as a scaling vector).

Our approach leverages 3DGS's key feature: representing scenes as a set of 3D Gaussians, each equivalent to an ellipsoid. This representation forms the foundation of our method.

Cage-based Deformation To deform a fine mesh using a cage, we consider a cage $\mathcal{C}_s$ with vertices $\{\mathbf{v}_j\}$. Points $\mathbf{x} \in \mathbb{R}^3$ inside the cage $\mathcal{C}_s$ can then be represented by cage coordinates $\{\omega_j\}$ (e.g., mean value coordinates [33]). These coordinates define the position of $\mathbf{x}$ relative to the cage vertices. The position of $\mathbf{x}$ is calculated as the weighted sum of cage vertex positions:

$$\mathbf{x} = \sum_j \omega_j \mathbf{v}_j \tag{1}$$

After deforming the cage from $\mathcal{C}_s$ to $\mathcal{C}_d$ with vertices $\{\mathbf{v}'_j\}$, we can compute the new position $\mathbf{x}'$ of $\mathbf{x}$ using the calculated cage coordinates:

$$\mathbf{x}' = \sum_j \omega_j \mathbf{v}'_j \tag{2}$$

The cage defines a continuous field within its boundaries, allowing it to deform the enclosed fine mesh by manipulating its vertices. This deformation process also works for arbitrary points within the source cage.

B. Cage-Building Algorithm

Algorithm 1 Cage-Building Algorithm

```
Require: 3DGS Scene $S$, config parameters (num_rings $n_r$,
         cameras_per_ring $n_c$, expand factor $s$)
Ensure: Simplified Cage Mesh $C$
  ▷ compute expanded bounding sphere ◁
  $M$ = means of Gaussians in $S$
  $m$ = Mean($M$)
  $r$ = Max(L2 distance from points in $M$ to $m$) * $s$
  ▷ generate cameras surrounding S, with top and bottom ◁
  $A$ = EmptyList()
  for $\phi$ in $[0, \frac{2\pi}{n_c}, \frac{4\pi}{n_c}, ..., 2\pi, 0, \pi]$ do
      for $\theta$ in $[\frac{\pi}{n_r+2}, \frac{2\pi}{n_r+2}, ..., \frac{n_r\pi}{n_r+2}, 0, 0]$ do
          $x = r\sin(\theta)\cos(\phi)$
          $y = r\sin(\theta)\sin(\phi)$
          $z = r\cos(\theta)$
          $a$ = camera at position $x, y, z$, looking at $m$
          A.append($a$)
  ▷ render depth image ◁
  $D$ = Render3DGS($S$, $A$)
  ▷ reconstruct voxel grid ◁
  $F_{tsdf}$ = TSDFIntegration($D$, $A$)
  $V_s$ = ExtractSurfaceVoxel($F_{tsdf}$)
  $D_{clean}$ = RenderTSDF($F_{tsdf}$, $A$)
  $V_i$ = DepthCarving($D_{clean}$, $A$)
  $V$ = merge voxels in $V_s$ and $V_i$
  ▷ smooth and simplify ◁
  $V_b$ = MorphoClosing($V$)
  $C_{raw}$ = MarchingCube($V_b$)
  $C_s$ = BilateralFilter($C_{raw}$)
  $C$ = EdgeCollapse($C_s$)
  return $C$
```

Cage-based deformation requires a cage mesh to function. Given a trained 3DGS (or its variants) model $\mathcal{S}_s$, our automated cage-generation algorithm aims to create a simple cage

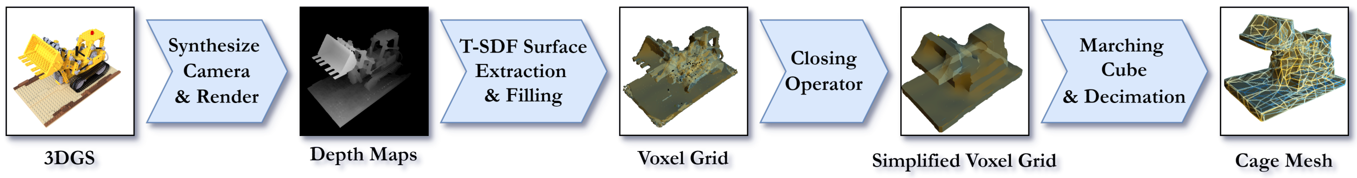
3DGS
Synthesize Camera & Render
Depth Maps
T-SDF Surface Extraction & Filling
Voxel Grid
Closing Operator
Simplified Voxel Grid
Marching Cube & Decimation
Cage Mesh

Fig. 1. Overview of our cage-building algorithm. Given an object, our method renders depth image from it, performs T-SDF integration, surface extraction and space carving to produce a solid voxel grid. The voxel grid is then simplified using morphological closing operator, meshed using marching cube, and decimated to obtain the final cage mesh.

$\mathcal{C}_s$ that encloses it. This cage can then be modified to enable deformation.

Existing methods, such as CageNeRF [3] and DeformingNeRF [2], use a marching-cube-then-simplify approach for cage building: they treat 3DGS as an opacity field, apply marching cubes to generate meshes, and then simplify these meshes to create the final cage. However, this approach struggles with noise and artifacts in trained 3DGS models, particularly floaters. Moreover, it is not applicable to 3DGS variants that use non-volumetric primitives, such as 2DGS [9], which represents scenes using flat 2D planes as primitives. As shown in the red-circled areas of Figure 4, this approach produces disconnected and floating small pieces due to floaters and artifacts in 3DGS, and it fails entirely for 2DGS. Our method overcomes these limitations.

Unlike existing methods, our render-reconstruct-simplify approach, illustrated in Figure 1, uses depth map renders to extract geometry. We leverage KinectFusion's truncated signed distance field (T-SDF) integration algorithm [34] to convert these depth maps into a T-SDF volume. This process effectively eliminates spurious geometries caused by artifacts in 3DGS models, particularly floaters. Additionally, this depth map-based approach makes our method applicable to non-volumetric 3DGS variants, such as 2DGS. The T-SDF volume undergoes surface extraction and depth carving to produce a solid voxel grid. We then simplify this grid using the morphological closing operator [32], followed by final mesh conversion and cage simplification. Algorithm 1 provides the pseudocode for our algorithm.

In summary, our method enhances cage extraction by utilizing depth maps for geometry information and combining T-SDF integration with morphological closing. This approach effectively addresses floaters and artifacts in 3DGS models and supports non-volumetric 3DGS variants.

C. Deformation Algorithm

Our deformation algorithm takes a trained 3DGS scene $\mathcal{S}_s$ along with source and target cages, $\mathcal{C}_s$ and $\mathcal{C}_d$. These cages define a deformation for part or all of the scene. The objective is to produce the deformed scene $\mathcal{S}_d$, a 3DGS representation with the specified deformation applied.

The algorithm performs deformation on the 3D Gaussians that constitute the 3DGS scene representation. For each Gaussian s with mean $\mu_s \in \mathbb{R}^3$ and covariance $\mathbf{\Sigma}_s \in \mathbb{M}^{3x3}$ (encoded by a rotation matrix $\mathbf{R}$ and scaling matrix $\mathbf{S}$), our deformation process is applied. This process is illustrated in Figure 2. For a detailed algorithmic description, please refer to the pseudocode provided in Appendix A.

To Ellipsoid To geometrically manipulate the 3D Gaussians, we start by converting them into explicit geometries, namely ellipsoids. The ellipsoids are represented using point clouds so they can be deformed by cage-based deformation.

According to 3DGS [1], a 3D Gaussian with mean μ_s and covariance $\mathbf{\Sigma}_s$ is defined as:

$$G(x) = \exp\left\{-\frac{1}{2}(\mathbf{x}-\mu_s)^\mathsf{T}\mathbf{\Sigma}_s^{-1}(\mathbf{x}-\mu_s)\right\}$$

The ellipsoid is then defined in quadric form as:

$$(\mathbf{x}-\mu_s)^\mathsf{T}\mathbf{\Sigma}_s^{-1}(\mathbf{x}-\mu_s) = 1$$

Here, μ_s is the ellipsoid's center $\mathbf{c}$. The principal axes and their lengths are derived from the eigenvalue decomposition of $\mathbf{\Sigma}_s^{-1}$, that is;

- The three principal axes (e.g., x, y, z) correspond to the eigenvectors.
- The axis lengths are inversely proportional to the eigenvalues of $\mathbf{\Sigma}_s^{-1}$.

We define six intersection points of the ellipsoid's principal axes with its surface as:

$$AP = \{\mathbf{c}, \mathbf{x_1}, \mathbf{y_1}, \mathbf{z_1}, \mathbf{x_2}, \mathbf{y_2}, \mathbf{z_2}\} \tag{3}$$

where $\mathbf{x}_{1,2}$ denote the two intersection points on the x-axis, with similar definitions for y and z. These points, AP, describe the ellipsoid and form a proxy point cloud for cage-based deformation.

Deform Points with Cages With the proxy point cloud AP_s in place, we apply the desired deformation defined by the source cage $\mathcal{C}_s$ and target cage $\mathcal{C}_d$ to it.

More concretely, we transform AP_s using Mean Value Coordinates (MVC) [23]. First, we convert AP_s from Euclidean coordinates to MVC using $\mathcal{C}_s$. Then, we convert them back to Euclidean coordinates using $\mathcal{C}_d$. The resulting deformed axis points are denoted as AP_d.

Transform Gaussians With the original and deformed points, we then estimate the underlying transformation and apply it to the original 3D Gaussians s.

Given the original and deformed points AP_s and AP_d, we compute the transformation $\mathbf{T} \in \mathbb{R}^{3\times3}$ by minimizing:

$$\min_{\mathbf{T}} \|\mathbf{D}_d - \mathbf{T}\mathbf{D}_s\|^2 \tag{4}$$

where $\mathbf{D} = [\mathbf{x_1}-\mathbf{c}, \mathbf{y_1}-\mathbf{c}, \mathbf{z_1}-\mathbf{c}, \mathbf{x_2}-\mathbf{c}, \mathbf{y_2}-\mathbf{c}, \mathbf{z_2}-\mathbf{c}] \in \mathbb{R}^{3\times6}$ for AP_s or AP_d. The least squares solution for T is given by:

$$\mathbf{T} = \mathbf{D}_d\mathbf{D}_s^\mathsf{T}(\mathbf{D}_s\mathbf{D}_s^\mathsf{T})^{-1} \tag{5}$$

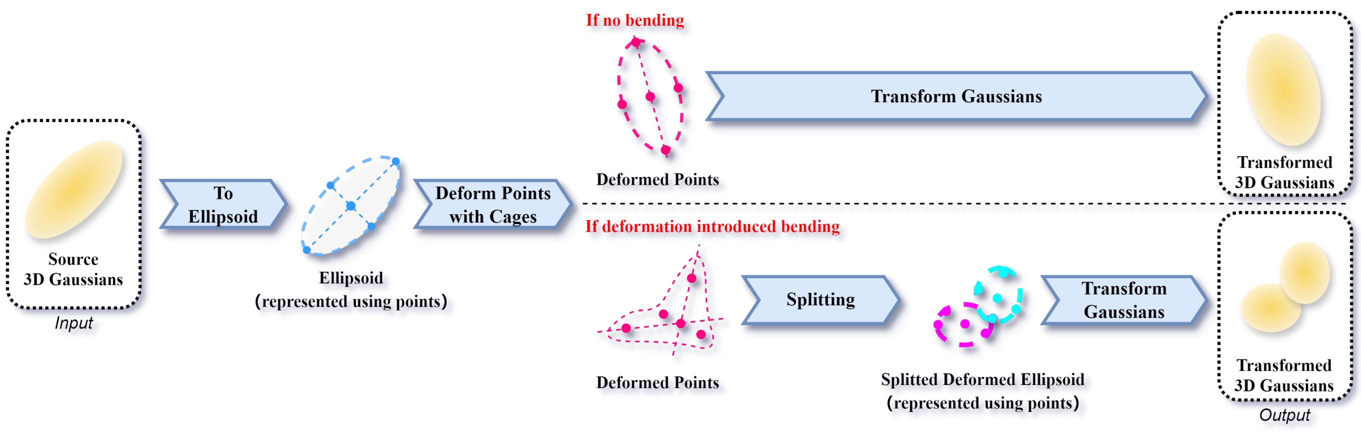

Fig. 2. Overview of our deformation algorithm. The deformation process is shown in 2D for clarity. For deformation, 3DGS Gaussians are converted to ellipsoids represented using points (the proxy point cloud). Proxy points are deformed using cage-based deformation and split if their axes are bent. Finally, deformed points are used to infer transformations for the Gaussians. For more details, please refer to the pseudo-code in Appendix A.

The 3D Gaussian s can then be transformed using $\mathbf{T}$, while using the center of deformed points AP_d as the new mean:

$$\mu_d = \mathbf{c}_d \tag{6}$$

$$\mathbf{\Sigma}_d = \mathbf{T}\mathbf{\Sigma}_s\mathbf{T}^\mathsf{T} \tag{7}$$

This step is crucial to our algorithm as it updates the Gaussians' covariance, which models their shape and orientation. Not updating covariance would lead to severe artifacts, which we will demonstrate in ablation studies.

According to the implementation of 3DGS [1], the transformed mean and covariance can be directly used for rendering. Optionally, to recover rotation and scaling from the covariance, use SVD decomposition $\mathbf{\Sigma}_d = \mathbf{U}\mathbf{\Sigma}\mathbf{V}^\mathsf{T}$, where $\mathbf{U}$ gives rotation and $\sqrt{\mathbf{\Sigma}}$ gives scaling.

Splitting Cage-based deformation enables flexible shape manipulation but introduces non-rigid warping, requiring some Gaussians to bend in deformation. This leads to visual artifacts since a single transformed Gaussian cannot properly represent these bent shapes. To address this, we split the bent Gaussians into multiple well-formed Gaussians to approximate the bent shapes.

We start by identifying the bent Gaussians to split. Given a Gaussian with deformed points AP_d, its center is $\mathbf{c}'_d \in AP_d$. The deformed points of an axis (e.g., x-axis) are $\mathbf{x}'_1, \mathbf{x}'_2 \in AP_d$. We calculate the angle between vectors, $\mathbf{x}'_1 - \mathbf{c}'$ and $\mathbf{x}'_2 - \mathbf{c}'$. Splitting is required if the angle falls below a threshold.

The splitting method divides a pre-MVC Gaussian ellipsoid into two smaller ellipsoids along a chosen axis. Each new ellipsoid has its axis lengths reduced by factor k, and both are positioned to meet at the center of the original ellipsoid along the splitting axis. Finally, both resulting ellipsoids undergo MVC transformation again for further processing. The resulting two smaller ellipsoids are more tolerable to deformation along that axis, reducing the risk of bending or distortion when applying MVC directly to elongated shapes.

We determine the axis scaling factor k by analyzing the optimal value that can maximally preserve the volume and shape of the original ellipsoid. More concretely, our scaling factor should satisfy two key constraints: Volume Preservation and Shape Preservation.

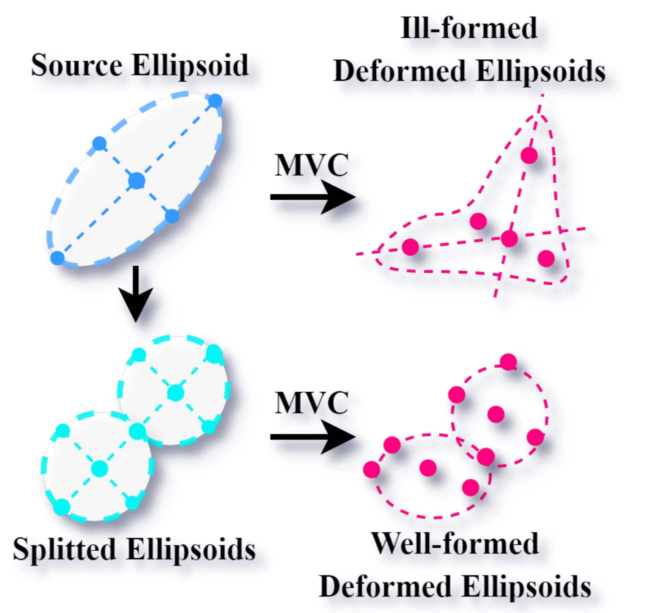
Source Ellipsoid
Ill-formed Deformed Ellipsoids
MVC
MVC
Splitted Ellipsoids
Well-formed Deformed Ellipsoids

Fig. 3. The splitting process. Our method fixes the ill-formed bent Gaussian by splitting the Gaussian before MVC deformation, leading to well-formed Gaussians and, thus, reasonable transforms.

Volume Preservation Constraint: The volume of the two smaller ellipsoids combined should approximate the volume of the original ellipsoid. This can be expressed as:

$$L_V = \frac{2}{3}\pi abc - 2\frac{2}{3}\pi k_1 a k_2 b k_3 c \tag{8}$$

where, a, b, c are the semi-principal axes of the original ellipsoid, k_1, k_2, k_3 are the individual scaling factors for the smaller ellipsoids. Simplifying this equation leads to:

$$k_1 k_2 k_3 = \frac{1}{2} \tag{9}$$

Shape Preservation Constraint: Each smaller ellipsoid should maintain a shape similar to the original ellipsoid. This constraint can be expressed as:

$$\frac{k_1 a}{k_2 b} \approx \frac{a}{b} \quad \frac{k_2 b}{k_3 c} \approx \frac{b}{c} \quad \frac{k_1 a}{k_3 c} \approx \frac{a}{c} \tag{10}$$

From these constraints, the scaling factor for all axes becomes:

$$k_1 = k_2 = k_3 = \sqrt[3]{\frac{1}{2}} \tag{11}$$

Thus, the scaling factor k for splitting should be $\sqrt[3]{\frac{1}{2}}$.

In practice, setting $k = \frac{1}{2}$ produces marginally better results, as demonstrated by our ablation study.

In summary, our algorithm deforms 3DGS by first converting 3D Gaussians into ellipsoids represented using points. Deformations of the points can then be transferred back to the underlying 3D Gaussians. This approach directly operates on the primitives of 3DGS, thus no architectural changes or retraining is needed. Furthermore, with caching, this direct transform approach can work in real-time. Finally, since it operates directly on the primitives, our method can be easily extended to work with 3DGS variants without concerns on training (such as FLoD [35]) and integrate with other 3DGS editing work (such as GaussianEditor [10]) with minimal changes.

Remark We propose a splitting procedure to handle non-rigid warping that bends Gaussians. This approach improves deformation quality for scenes with intricate details, especially when a single Gaussian representing a straight surface must be bent. Unfortunately, the existing methods, such as ARAP-GS [22] and VR-GS [8], ignore this issue.

IV. Experiments

A. Implementation Details

For cage building, the voxel grid's resolution is set to 128. We employ the T-SDF integration and carving procedure from Open3D [36], using their default parameters.

For deformation, we set the splitting threshold at 175 degrees and avoid splitting axes with lengths below 1e-2 for numerical stability. For cages that only encompass part of the scene, we compute the convex hull of the cage and only deform gaussians fall inside it for speed and stability.

We ran all experiments using an NVIDIA A5000 GPU and an AMD Ryzen Threadripper PRO 3975WX processor (32 cores).

B. Cage Building Quality

Our evaluation begins by analyzing the effectiveness and extensibility of our cage-building algorithm.

We evaluate our approach against the traditional marching-cube-then-simplify process used in NeRFShop [4] and DeformingNeRF [2]. However, since the process used by existing methods is designed for radiance fields and cannot directly work with 3DGS, we adapt them based on SuGaR's [13] approach, as detailed in Appendix Section B. Additionally, we test a variant of this baseline that uses our voxel grid smoothing and simplification process instead of direct edge collapse to highlight the strength of our render-reconstruct design.

We evaluate both methods using the Lego scene from the NeRF Synthetic Dataset [37] and a flower vase extracted from the MipNeRF360 Dataset's garden scene [38].

In Figure 4, we compare the output of our method with the marching cube (MC) baseline, showing both the raw voxel grids (before any smoothing operation) and the final meshes. Our method yields cleaner voxel grids for Lego and vase scenes, leading to higher-quality cages. In contrast, the baseline's noisy voxel grids lead to highly dense and noisy mesh that cannot be used. Even using our smoothing and simplification process, the MC baseline still creates unwanted bubbles in the Lego cage and complex edges in the vase cage.

Our cage-building algorithm also extends naturally to 3DGS variants. When applied to a trained 2DGS representation of the vase (third row of Figure 4), the MC baseline method fails to produce a coherent voxel grid and cage. Even with our voxel grid smoothing process, the cage is still hollow, while our approach still generates accurate voxel grids and cages suitable for cage-based deformation. This difference occurs because 2DGS uses flat 2D ellipses with minimal volume instead of volumetric 3D ellipsoids. Our method remains effective regardless of this distinction.

C. Deformation Quality

We then compare the deformation quality of our model against existing methods on the NeRF Synthetic Dataset [37]. We start with pre-trained 3D Gaussian Splatting [1] models, apply our cage construction algorithm for cages, manually deform the cages, and run our deformation algorithm. For comparison, we train and deform DeformingNeRF [2], GaMeS [5], SuGaR [13], and Gaussian Frosting [6] on the same objects as well. We use our cage to deform their underlying mesh or triangle soup for fair comparisons.

Normal Deformations We present our results in Figure 5. In the microphone scene, DeformingNeRF fails to preserve the detailed grid structure of the microphone's mesh, while Gaussian Frosting produces holes and spiky artifacts on it. GaMeS and SuGaR also show spiky artifacts. For the ficus scene, DeformingNeRF and Gaussian Frosting create artifacts on the unedited flower pot. In the expanded upper part, Gaussian Frosting and SuGaR struggle with details, breaking connections between branches. In the hotdog scene, there are wrinkles on the plate with DeformingNeRF, severe tearing with Gaussian Frosting, and spiking artifacts with SuGaR and GaMeS due to the lack of a splitting process. Across all scenes, our approach is the only method that consistently produces the smoothest and most plausible results.

Extreme Deformations We further test how well these methods handle challenging deformations. In Figure 6, we rotate the bulldozer's head in the Lego scene from the NeRF Synthetic Dataset by 90, 135, and 180 degrees. As can be seen, DeformingNeRF fails to handle twisting. Gaussian Frosting produces blurry artifacts across all angles. GaMeS shows spiky artifacts. While SuGaR works reasonably well at 90 degrees,

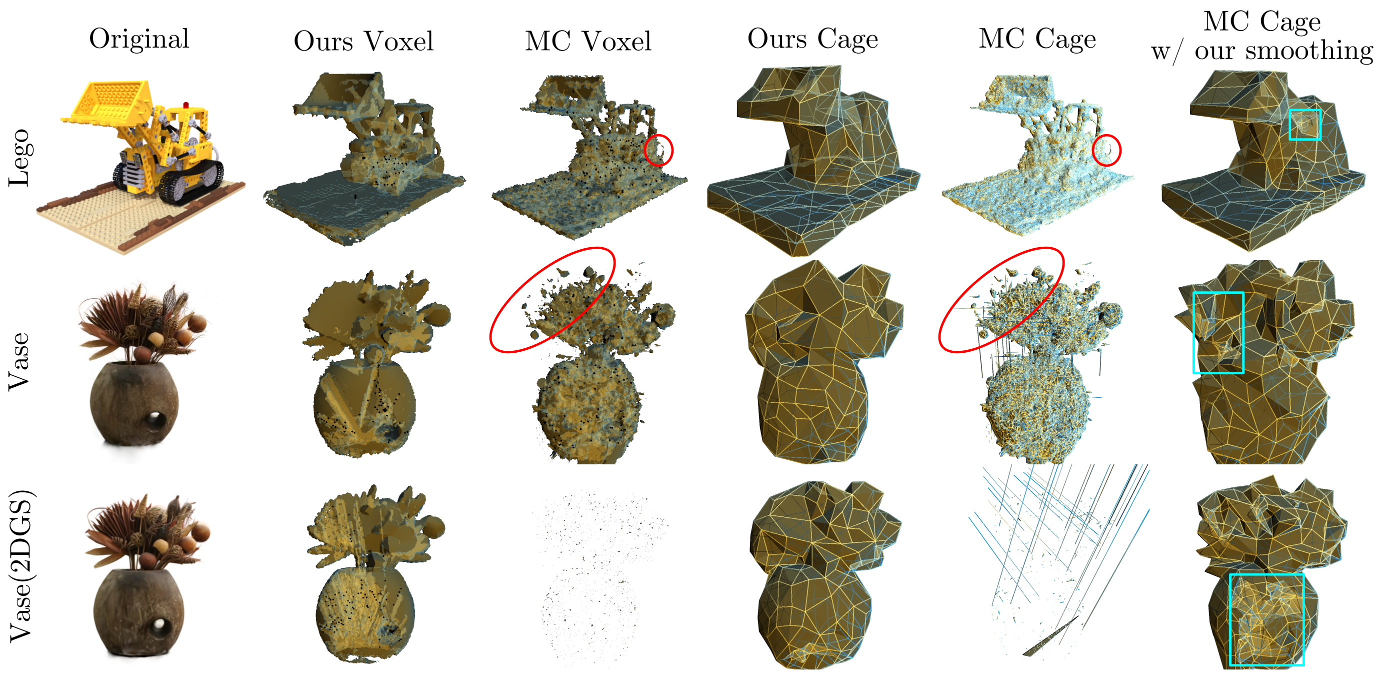

Fig. 4. Comparison of cage building algorithm. We present the raw voxel grids and the produced final cages for comparison. **Red circles** and **cyan boxs** marks defects. Note that our method generates cleaner voxel grids and smoother final cages for both 3DGS and 2DGS. The marching cube(MC) baseline generates overly dense mesh for 3DGS scenes and **completely fails** on 2DGS scenes. Our smoothing process enabled it to produce coherent results, but artifacts remain.

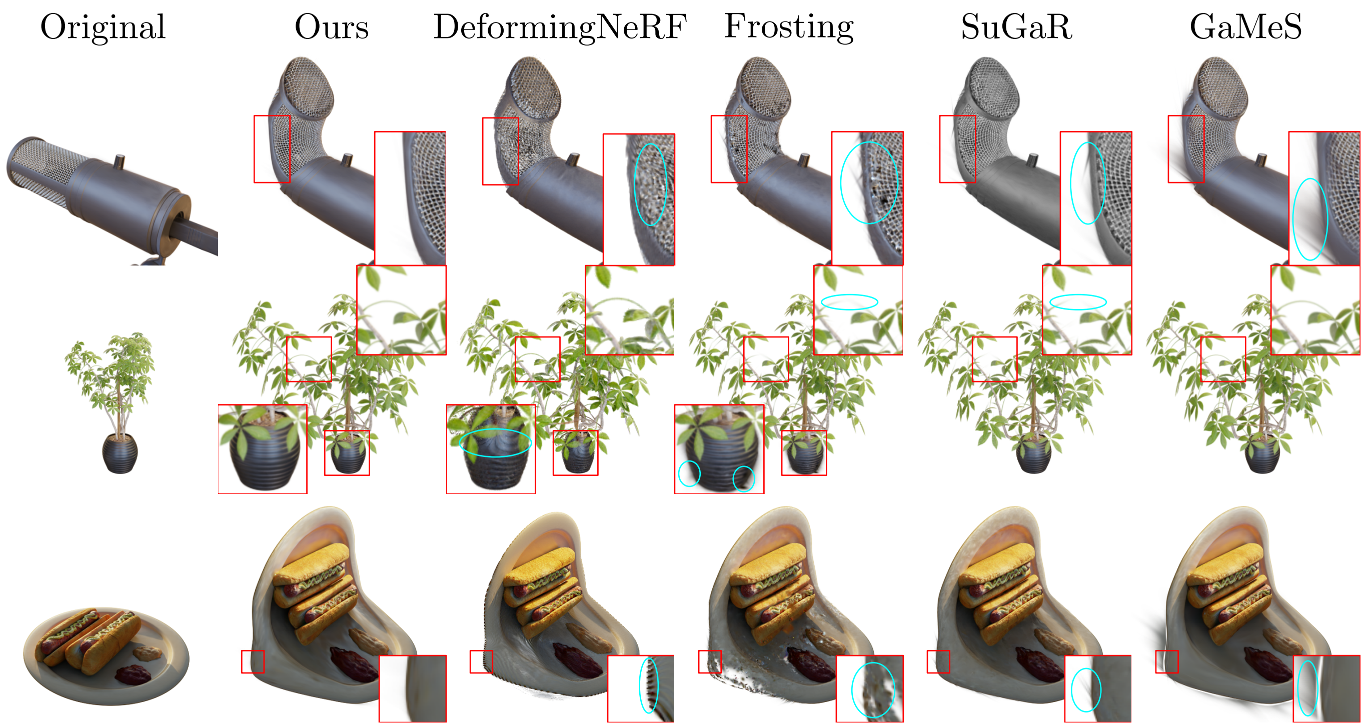

Fig. 5. Comparison of methods on selected objects. **Red boxes** indicate zoomed areas; **cyan circles** marks defects. Not having defect marks indicates satisfactory results. Our approach is the only method that performs well across all cases. For more results, refer to our supplementary video.

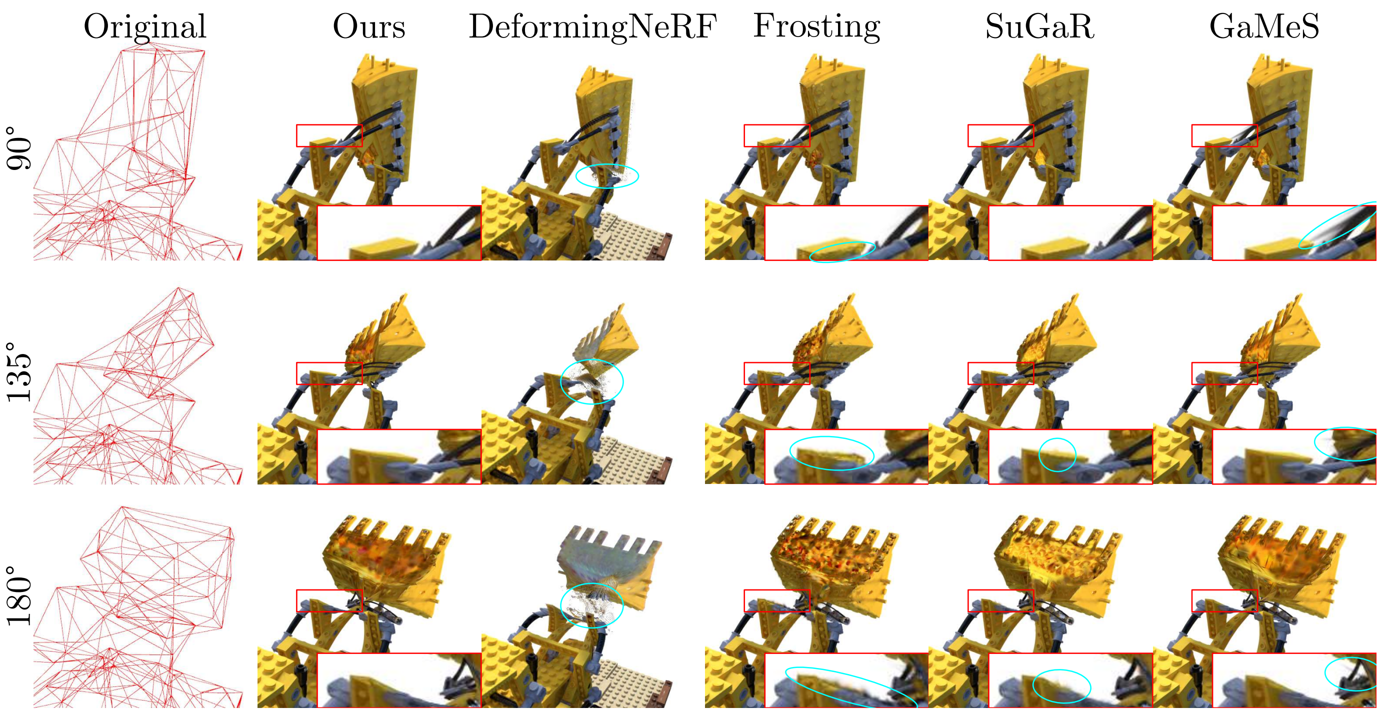

Fig. 6. Comparison of methods from normal to extreme deformations. **Red boxes** indicate zoomed areas; **cyan circles** marks defects. Not having defect marks indicates satisfactory results. Note that our method remains robust as deformation intensifies, while other methods develop artifacts. Even under the 180-degree extreme scenario, our method still produces reasonable results.

it creates artifacts at larger angles. In contrast, our method remains stable and generates reasonable results even under extreme rotations.

D. Other Control Methods

Our method controls 3DGS deformation using triangular mesh cages, unlike VR-GS [8], which uses dense tetrahedral grids, and SC-GS [7], which uses sparse control points. Compared to these approaches, our triangular mesh approach is simpler and easier to integrate with existing 3D software or animation pipeline, and it achieves comparable, if not superior, quality in deformation.

Since VR-GS and SC-GS are designed for different scenarios, we adapt them for deformation by directly manipulating their control structure. We evaluate these approaches against our method using three scenes from the D-NeRF [39] dataset: mutant, jumpingjacks, and lego. For fair comparison, we train SC-GS on these dynamic scenes and extract models at a single time frame for testing VR-GS and our method. This is because SC-GS requires training on video data, while other methods do not. We then analyze each method's control structure for controlling deformation and deformation results.

As shown in Figure 7, our method controls deformation using standard triangle meshes, while VR-GS uses dense tetrahedral grids and SC-GS uses sparse control points. Our approach offers a simpler structure than VR-GS's simulation-focused design, and integrates better with existing animation software than both SC-GS and VR-GS. In terms of result quality, our method demonstrates clear advantages over SC-GS, producing smoother shoulder deformations in the jumpingjacks and mutant scenes, while avoiding the disconnection artifacts present in the lego scene. When compared to VR-GS, our method produces smoother details on the lego and jumpingjacks scenes, and the results are comparable in the mutant scene. This shows that our method is more effective in handling complex deformations while using a simpler and easier-to-integrate control method.

E. Training & Deformation Speed

We then benchmark the training and deformation times across all methods. We test on two sets of scenes/cages:

NeRF Scenes/Cages We select scenes from the NeRF Synthetic Dataset [37] and use the cages from our cage construction algorithm for deformation. The selected scenes are: lego, chair, ficus, and hotdog.

DeformingNeRF Scenes/Cages We also test on the scenes selected by DeformingNeRF [2], using DeformingNeRF's cages as well. More concretely, DeformingNeRF [2] selected two scenes from the NeRF Synthetic Dataset [37](chair and lego) and two from the NSVF [40] Synthetic Dataset (robot and toad).

We chose the ficus and hotdog scene over the robot and toad scene to test the method's performance when scaling objects with significant details or splitting Gaussians representing flat surfaces. In terms of cages, our cages are automatically generated and undergo extensive deformations, while DeformingNeRF's cages are manually created and have milder deformations.

Training Speed Table I presents the average training time for all methods, while the detailed per-scene results are shown in Table II. Training times of vanilla 3DGS are provided

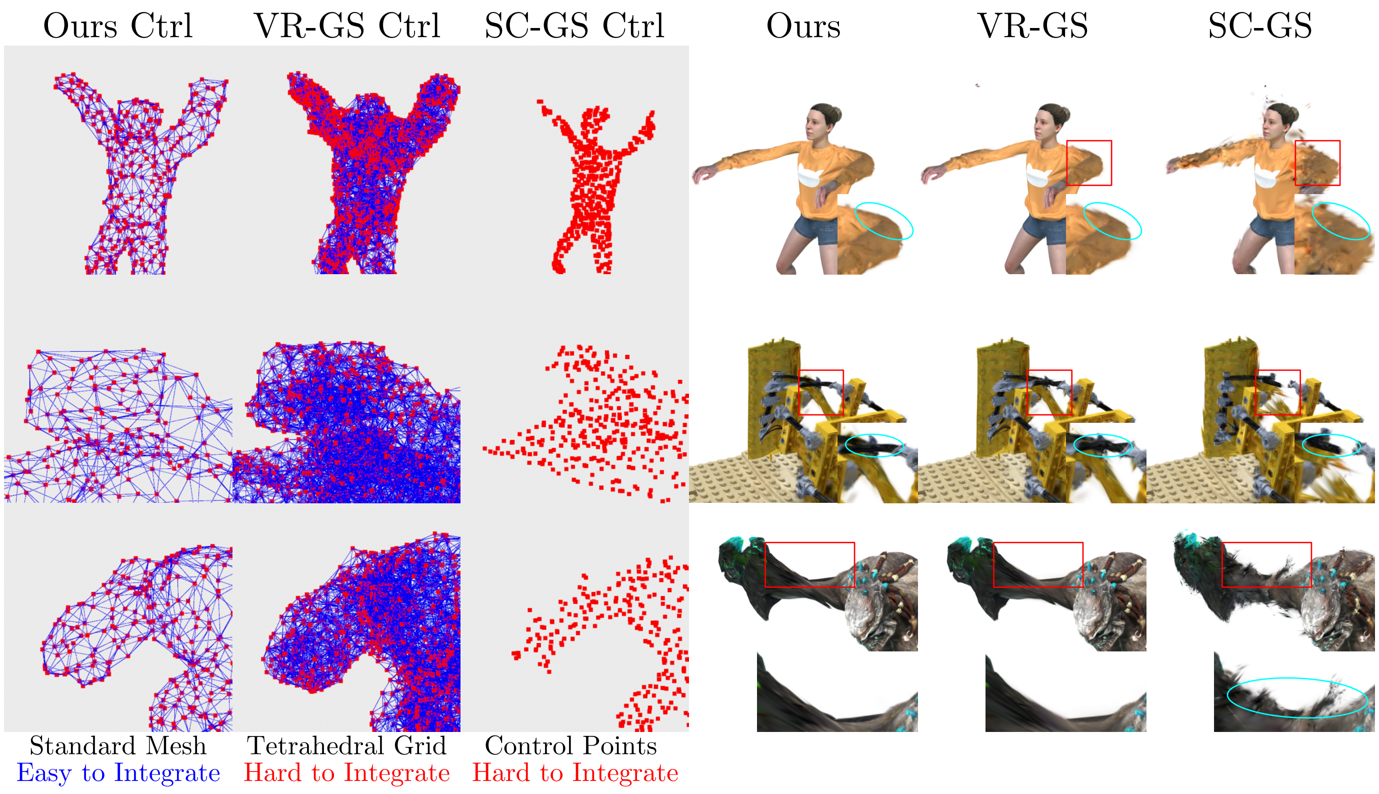

Fig. 7. Comparison with methods that can be adapted for deformation. We show the method's control structures and their output. Cyan circles mark defects, not having cyan circles indicates satisfactory results. Our method uses triangle mesh cages for control, which is simpler and easier to integrate with existing animation software such as Blender, unlike VR-GS or SC-GS. Our method also produces superior results. While VR-GS performed adequately on the mutant scene, it struggled with the lego scene's detailed deformations.

Method	NeRF [37] Scenes training (sec↓)	DeformingNeRF [2] Scenes training (sec↓)
DeformingNeRF [2]	491.33	479.18
SuGaR [13]	3234.30	3166.88
GaMeS [5]	**432.02**	**469.65**
Frosting [6]	2649.78	2673.52
Vanilla 3DGS [1]	**460.19**	**462.38**
Ours	**N/A**	**N/A**

TABLE I
BENCHMARK RESULTS COMPARING TRAINING TIMES. RED INDICATES BEST VALUES, BLUE MARKS SECOND-BEST. NOTE THAT WITH A PRE-TRAINED VANILLA 3DGS MODEL, OUR METHOD CAN DIRECTLY DEFORM IT WITHOUT RETRAINING OR CONVERSION.

for reference. With a pre-trained vanilla 3DGS model or its variants, our method can directly deform it without retraining or conversion, hence no training would be needed. In contrast, other approaches require retraining or conversion because they altered the architecture of 3DGS for editability.

Deformation Speed Table III presents the average deformation time for all methods, and the detailed per-scene results are provided in Table IV and Table V. As Table III presents, our method, on average, achieves 60FPS on the simpler DeformingNeRF cages and our more challenging cages, hence real-time deformation. In terms of once-per-scene preprocessing, our approach is slower compared to mesh-based 3DGS methods like SuGaR [13], GaMeS [5], and Gaussian Frosting [6]. This is because our method needs to process

NeRF [37] Scenes			DeformingNeRF [2] Scenes		
Scene	Method	training (sec↓)	Scene	Method	training (sec↓)
chair	DeformingNeRF [2]	451.15	chair	DeformingNeRF [2]	451.15
	SuGaR [13]	3154.14		SuGaR [13]	3154.14
	GaMeS [5]	**427.86**		GaMeS [5]	**427.86**
	Frosting [6]	2651.98		Frosting [6]	2651.98
	Vanilla 3DGS [1]	**417.16**		Vanilla 3DGS [1]	**417.16**
	Ours	**N/A**		Ours	**N/A**
lego	DeformingNeRF [2]	515.22	lego	DeformingNeRF [2]	515.22
	SuGaR [13]	3264.54		SuGaR [13]	3264.54
	GaMeS [5]	**462.17**		GaMeS [5]	**462.17**
	Frosting [6]	2726.72		Frosting [6]	2726.72
	Vanilla 3DGS [1]	**457.76**		Vanilla 3DGS [1]	**457.76**
	Ours	**N/A**		Ours	**N/A**
hotdog	DeformingNeRF [2]	621.38	robot	DeformingNeRF [2]	439.98
	SuGaR [13]	3475.71		SuGaR [13]	3060.61
	GaMeS [5]	**401.03**		GaMeS [5]	**407.78**
	Frosting [6]	2606.45		Frosting [6]	2603.48
	Vanilla 3DGS [1]	**535.54**		Vanilla 3DGS [1]	**400.25**
	Ours	**N/A**		Ours	**N/A**
ficus	DeformingNeRF [2]	**377.58**	toad	DeformingNeRF [2]	**510.36**
	SuGaR [13]	3042.79		SuGaR [13]	3188.21
	GaMeS [5]	437.01		GaMeS [5]	580.80
	Frosting [6]	2613.99		Frosting [6]	2711.88
	Vanilla 3DGS [1]	**430.30**		Vanilla 3DGS [1]	**574.36**
	Ours	**N/A**		Ours	**N/A**

TABLE II
DETAILED PER-SCENE TRAINING TIME OF TABLE I. RED INDICATES BEST VALUES, BLUE MARKS SECOND-BEST. TRAINING TIMES OF VANILLA 3DGS ARE ALSO PROVIDED FOR REFERENCE.

Method	NeRF [37] Scenes (Automatic Cages)			DeformingNeRF [2] Scenes (Manual Cages)		
	preprocess (ms↓)	deform (ms↓/FPS↑)	render (ms↓/FPS↑)	preprocess (ms↓)	deform (ms↓/FPS↑)	render (ms↓/FPS↑)
DeformingNeRF* [2]	3530.10	3933.93 / 0.25FPS	4970.13 / 0.20FPS	2642.48	2420.32 / 0.41FPS	3441.58 / 0.29FPS
SuGaR [13]	**1197.03**	1483.37 / 0.67FPS	17.26 / 57.94FPS	**746.24**	1474.52 / 0.68FPS	16.78 / 59.59FPS
GaMeS [5]	1517.75	**8.34 / 119.90FPS**	**5.87 / 170.36FPS**	1183.13	**6.56 / 152.44FPS**	**6.24 / 160.26FPS**
Frosting [6]	**1163.60**	125.83 / 7.95FPS	17.27 / 57.90FPS	**715.36**	122.48 / 8.16FPS	16.62 / 60.17FPS
Ours	3565.11	**16.42 / 60.90FPS**	**4.12 / 242.72FPS**	2744.05	**12.33 / 81.10FPS**	**3.97 / 251.89FPS**

* DeformingNeRF performs deformation during rendering. Note that the render time involves the deformation time.

TABLE III
BENCHMARK RESULTS COMPARING DEFORMATION TIMES. RED INDICATES BEST VALUES, BLUE MARKS SECOND-BEST. DEFORMATION TIMES INCLUDE ONCE-PER-SCENE PREPROCESSING AND ACTUAL DEFORMATION. THE TIME TO RENDER THE DEFORMED REPRESENTATION IS ALSO PRESENTED HERE. OUR METHOD ACHIEVES REAL-TIME PERFORMANCE (∼60FPS) FOR BOTH CAGE TYPES AND IS THE FASTEST IN RENDERING.

Scene	Method	NeRF [37] Scenes		
		preprocess (ms↓)	deform (ms↓/FPS↑)	render (ms↓/FPS↑)
chair	DeformingNeRF [2]	3361.99	2882.62 / 0.35FPS	3908.45 / 0.26FPS
	SuGaR [13]	**1055.86**	1528.79 / 0.65FPS	17.04 / 58.69FPS
	GaMeS [5]	1355.31	**7.25 / 137.93FPS**	**5.42 / 184.50FPS**
	Frosting [6]	**1023.09**	125.62 / 7.96FPS	16.36 / 61.12FPS
	Ours	3124.88	**13.89 / 71.99FPS**	**3.43 / 291.55FPS**
lego	DeformingNeRF [2]	4075.17	4633.86 / 0.22FPS	5668.55 / 0.18FPS
	SuGaR [13]	**1510.96**	1511.84 / 0.66FPS	16.91 / 59.14FPS
	GaMeS [5]	2188.09	**12.09 / 82.71FPS**	**6.43 / 155.52FPS**
	Frosting [6]	**1495.65**	133.17 / 7.51FPS	16.10 / 62.11FPS
	Ours	5148.76	**23.71 / 42.18FPS**	**4.12 / 242.72FPS**
hotdog	DeformingNeRF [2]	3500.92	3989.47 / 0.25FPS	5028.07 / 0.20FPS
	SuGaR [13]	1234.86	1477.10 / 0.68FPS	17.46 / 57.27FPS
	GaMeS [5]	**803.10**	**4.43 / 225.73FPS**	**4.30 / 232.56FPS**
	Frosting [6]	**1156.40**	122.38 / 8.17FPS	17.01 / 58.79FPS
	Ours	1918.72	**9.53 / 104.93FPS**	**3.25 / 307.69FPS**
ficus	DeformingNeRF [2]	3182.31	4229.77 / 0.24FPS	5275.44 / 0.19FPS
	SuGaR [13]	**986.44**	1415.76 / 0.71FPS	17.61 / 56.79FPS
	GaMeS [5]	1724.51	**9.59 / 104.28FPS**	**7.34 / 136.24FPS**
	Frosting [6]	**979.27**	122.16 / 8.19FPS	19.61 / 50.99FPS
	Ours	4068.09	**18.53 / 53.97FPS**	**5.68 / 176.06FPS**

TABLE IV
DETAILED PER-SCENE DEFORMATION TIME OF TABLE III ON NERF SCENES. NOTE THAT OUR METHOD IS CONSISTENTLY THE SECOND-FASTEST IN DEFORMATION AND FASTEST IN RENDERING.

Scene	Method	DeformingNeRF [2] Scenes		
		preprocess (ms↓)	deform (ms↓/FPS↑)	render (ms↓/FPS↑)
chair	DeformingNeRF [2]	3422.40	2910.13 / 0.34FPS	3936.68 / 0.25FPS
	SuGaR [13]	**1061.50**	1486.58 / 0.67FPS	16.91 / 59.14FPS
	GaMeS [5]	1353.42	**7.49 / 133.51FPS**	**5.43 / 184.16FPS**
	Frosting [6]	**1018.24**	126.04 / 7.93FPS	16.98 / 58.89FPS
	Ours	3139.67	**14.31 / 69.88FPS**	**3.71 / 269.54FPS**
lego	DeformingNeRF [2]	2084.41	1197.90 / 0.83FPS	2219.81 / 0.45FPS
	SuGaR [13]	**441.99**	1532.87 / 0.65FPS	16.83 / 59.42FPS
	GaMeS [5]	593.17	**3.36 / 297.62FPS**	**6.17 / 162.07FPS**
	Frosting [6]	**424.85**	125.03 / 8.00FPS	15.84 / 63.13FPS
	Ours	1378.66	**6.18 / 161.81FPS**	**3.94 / 253.81FPS**
robot	DeformingNeRF [2]	1895.59	1441.66 / 0.69FPS	2440.74 / 0.41FPS
	SuGaR [13]	**517.81**	1421.84 / 0.70FPS	16.43 / 60.86FPS
	GaMeS [5]	706.71	**3.86 / 259.07FPS**	**5.68 / 176.06FPS**
	Frosting [6]	**510.92**	117.94 / 8.48FPS	17.00 / 58.82FPS
	Ours	1664.74	**7.19 / 139.08FPS**	**3.94 / 253.81FPS**
toad	DeformingNeRF [2]	3167.54	4131.60 / 0.24FPS	5169.09 / 0.19FPS
	SuGaR [13]	**963.66**	1456.78 / 0.69FPS	16.95 / 59.00FPS
	GaMeS [5]	2079.23	**11.51 / 86.88FPS**	**7.69 / 130.04FPS**
	Frosting [6]	**907.43**	120.92 / 8.27FPS	16.67 / 59.99FPS
	Ours	4793.12	**21.63 / 46.23FPS**	**4.29 / 233.10FPS**

TABLE V
DETAILED PER-SCENE DEFORMATION TIME OF TABLE III ON DEFORMINGNERF SCENES. NOTE THAT OUR METHOD IS CONSISTENTLY THE SECOND-FASTEST IN DEFORMATION AND FASTEST IN RENDERING.

more points for deformation and splitting, while mesh-based methods can simply deform the underlying mesh or triangle soup. However, our method is the fastest in rendering, as we use the unmodified vanilla 3DGS rendering process.

This can also be seen from the per-scene results shown in Table IV and Table V. As can be seen, our method is consistently the second-fastest in deformation and fastest in rendering.

V. APPLICATIONS

Our method can be extended to work with other methods or 3DGS variants, making it valuable for many application scenarios.

A. Composition and Animation

Since our deformation algorithm enables cage-based deformation on 3DGS, we can animate and compose different 3DGS models by animating their cages and placing the cages into another scene. This animation and composition can be done using existing mesh editing and animation software, such as Blender [41].

Figure 8 shows animated 3DGS versions of Mixamo [42] characters Sophie and Mutant, composited into the MipNeRF360 [38] garden scene. This is done by animating the cage of the characters using the automatic rigging and animation functionality of Mixamo, placing the cages within the garden scene, and applying our algorithm. As can be seen, our model achieves high-quality animation and composition of 3DGS models, which is useful for animators and artists intending to work with 3DGS.

B. Combining with Editing Methods

Our deformation algorithm achieves low-level, direct shape editing and can be integrated with other work on editing or editable 3DGS to complement their editing abilities.

We start by integrating with GaussianEditor [10], a text-prompt-based 3DGS editing method. As shown in Figure 9, in the face scene from the Instruct-NeRF2NeRF Dataset [44], we use GaussianEditor to select the scene's facial region and edit its appearance with the text prompt ”turn him into a clown”. We then apply our deformation algorithm to stretch the nose of the edited face. As can be seen, our method successfully stretched the nose of the edited face.

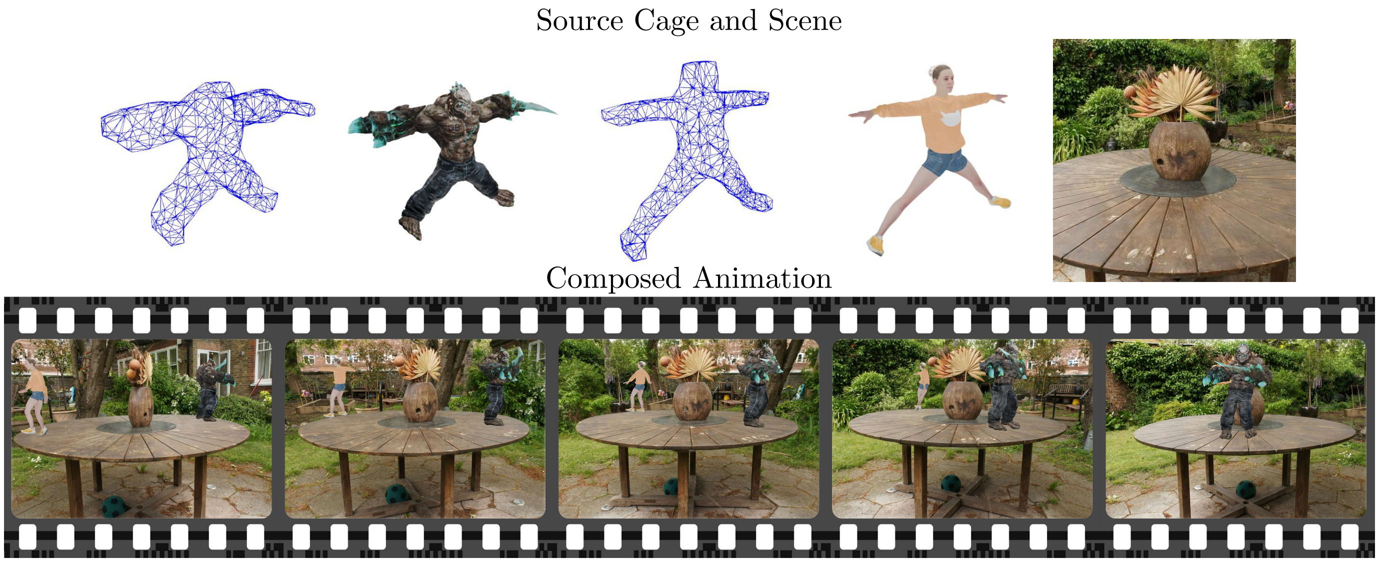

Fig. 8. Animating and composing scenes using our method. Note that our cage-based deformation algorithm can be used for animation and composition by animating the cages and placing the cages into another scene. Please refer to our supplementary video for more details.

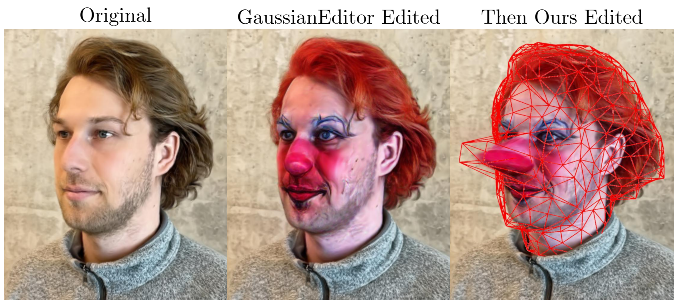

Fig. 9. Integrating our method with GaussianEditor [10]. Note that our approach successfully stretched the nose of the face edited by GaussianEditor. Please refer to our demo video for more results.

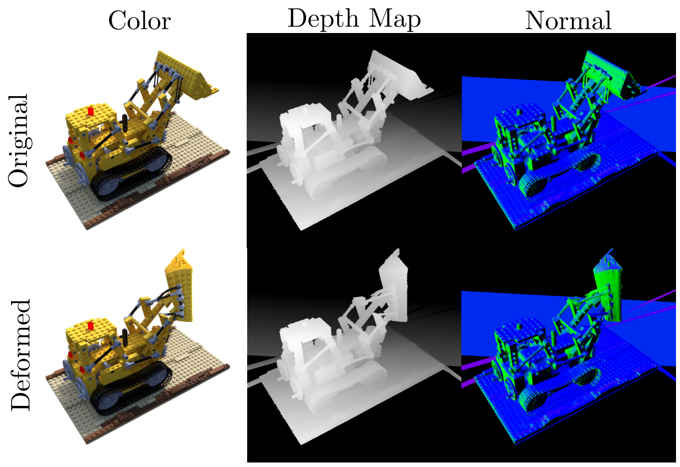

Fig. 11. Integrating our method with 2DGS [9]. Note that the deformation performed by our method is not only high-quality in RGB rendering but also in depth and normal map as well.

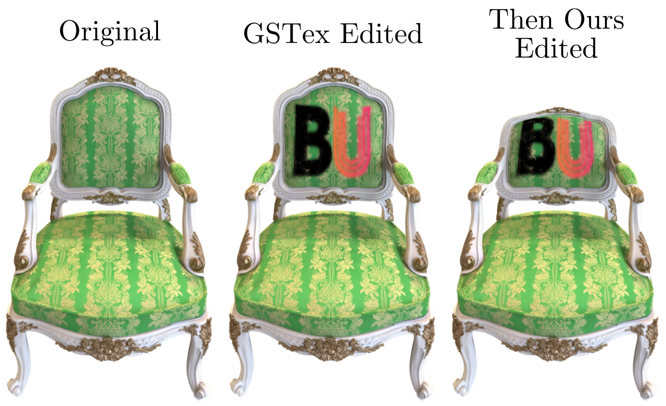

Fig. 10. Integrating our method with GSTex [43]. Note that GSTex enables texture editing, and our method enables shape editing combined to provide comprehensive editing capabilities.

Our method can also be integrated with GSTex [43], a 2DGS variant that allows texture editing. We tested this integration using a chair from the NeRF Synthetic Dataset [37]. As shown in Figure 10, we modified the chair's texture using GSTex, then applied our deformation algorithm to deform the result. This combination demonstrates how our approach enhances the overall editing capabilities.

C. Extending to Variants of 3DGS

Our method can also be extended to work with other 3DGS variants.

We start by integrating with 2DGS [9], a method that uses flattened 2D Gaussian disks instead of 3D Gaussian balls for improved geometry, depth rendering, and normal reconstruction. We demonstrate this by deforming a 2DGS capturing the lego scene from the NeRF Synthetic Dataset

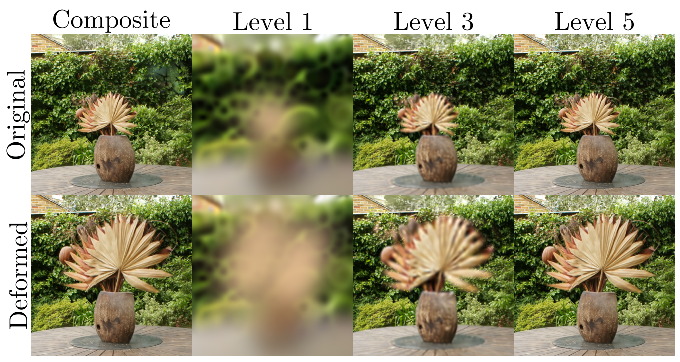

Fig. 12. Integrating our method with FLoD [35]. Our method enlarged the flowers, which is correctly applied to all Level-of-Details(LoD) levels and the final composite result.

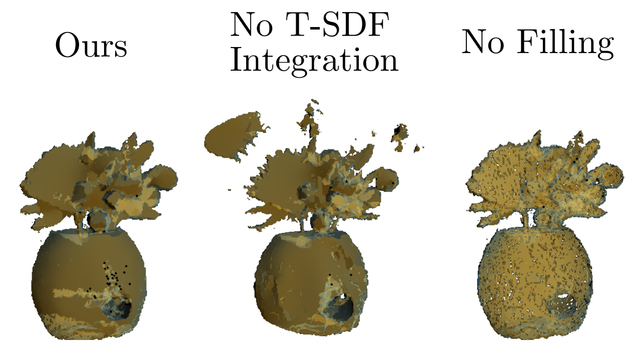

Fig. 13. Ablation study results for cage building algorithm. The voxel grids before closing simplification are shown. Note that not performing T-SDF integration would lead to artifacts on top of the vase, while not performing filling leads to porous and hollow shapes. Both would harm cage quality.

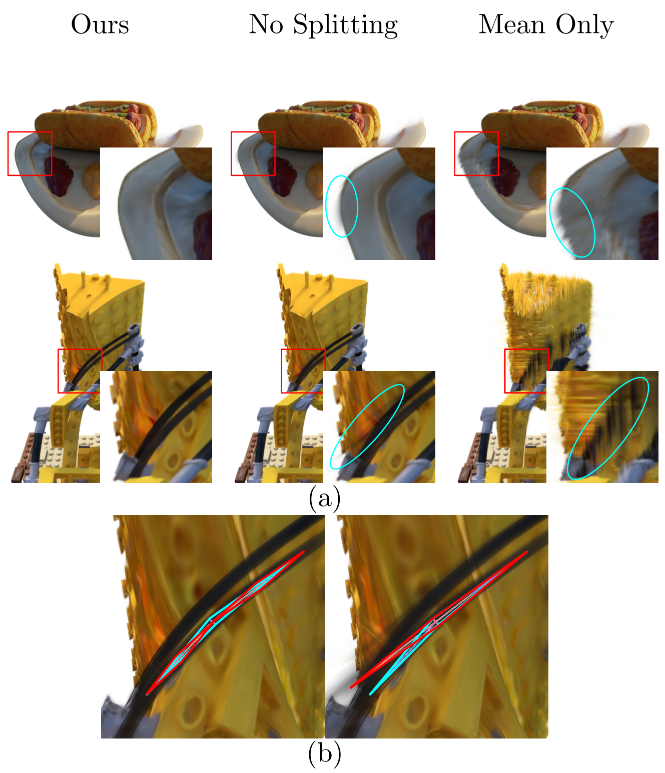

Fig. 14. (a) Ablation study results for deformation algorithm. Note the sharp spikes caused by disabling splitting in the highlighted area. The naive mean-only variant produces significant artifacts as well. (b) The zoomed-in view of (a) highlights the deformed Gaussian (**cyan diamond**) and the actual Gaussians (**red diamond**, including both splitting and non-splitting Gaussians). Note that when the deformed Gaussian is approximated using only one Gaussian, rather than splitting, noticeable spiking artifacts appear.

[37]. Results are shown in Figure 11; note the depth and normal render of the deformed model is high-quality as well.

We also integrate with FLoD [35], a method that adds Level-of-Details(LoD) to 3DGS. We test this by editing a FLoD capturing the garden scene from the MipNeRF360 dataset [38]. As shown by Figure 12, our deformation works well across all LoDs, demonstrating our method's adaptability to these variants of 3DGS. This adaptability could allow our method to utilize the available information across different models for different applications.

D. Ablation Studies

Cage-building Algorithm We start our ablation study by analyzing the key steps in our cage-building algorithm, using the vase segmented from the garden scene in the MipNeRF360 [38] dataset. We compare our voxel grid extraction method against two baselines: a naive approach that skips T-SDF integration and directly constructs voxel grids by performing depth carving using 3DGS-rendered depth maps (”No T-SDF Integration”), and a version of our algorithm that skips depth carving and use the surface points extracted from T-SDF integration instead (”No Filling”).

Figure 13 shows the produced voxel grids prior to applying the closing operator. Using depth maps directly for voxel carving without T-SDF integration creates noise on the vase's top. Without filling, the resulting voxel grid is porous and hollow, which closing operations cannot effectively remedy. Both approaches produce suboptimal results and could harm the cage's quality.

Deformation Algorithm To evaluate our design choices in the deformation algorithm, we compare our algorithm with two simpler variants: one without splitting and another that directly applies cage-based deformation to the position(mean) of the gaussians. We test these algorithms on the lego and hotdog scenes from the NeRF Synthetic Dataset [37]. Figure 14 shows the results.

As can be seen, the simpler mean-only variant of our algorithm produced significant striping artifacts. This is prevented in our algorithm by transforming the covariance (thus, rotation and shape) of the Gaussians as well. Furthermore, as shown in the highlighted and zoomed-in regions, using our algorithm without splitting results in spiking artifacts in bent regions. This occurs because the long belt is represented by a few thin, elongated ellipsoids. When bent, noticeable spiking artifacts appear, as shown in Figure 14 (b). Clearly, bending is challenging to approximate using a single Gaussian ellipsoid instead of splitting. This demonstrates that the splitting procedure is essential for handling large deformations. Simply optimizing the existing Gaussians, as proposed by ARAP-GS [22] or VR-GS [8], is insufficient for accurately modeling bending.

Split Scaling Factor Finally, we analyze our choice of scaling factor k in the splitting step using the Lego scene

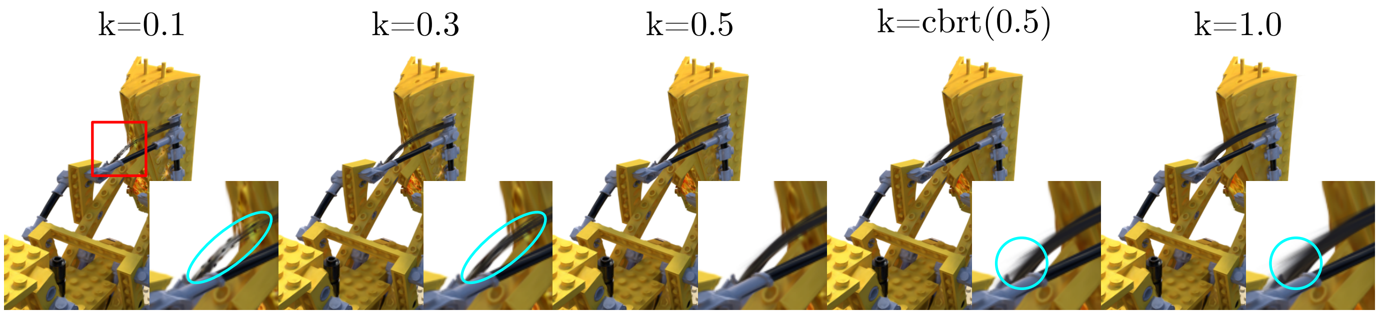

Fig. 15. Ablation study results for the split factor k. Note that setting k too low creates fragmented surfaces, while setting it too high results in sharp spikes. It is shown that 0.5 achieves a better balance than our theoretically derived value.

from the NeRF Synthetic Dataset [37].

As shown in Figure 15, the scaling factor k significantly impacts results. A large k (e.g., 1.0) creates spikes on the bulldozer's belt due to oversized split Gaussians failing to model the intricate bending deformation. Conversely, a small k (e.g., 0.1) produces fragmented surfaces as the split Gaussians become too small to cover the belt. While our theoretical analysis suggests k should be $\sqrt[3]{\frac{1}{2}}$ (denoted as cbrt(0.5)), empirically we find $\frac{1}{2}$ produces superior results.

VI. Conclusion

In this paper, we introduced GSDeformer, a cage-based deformation algorithm for 3D Gaussian Splatting (3DGS). Our approach can directly deform existing trained vanilla 3DGS in real time and can be easily extended to its variants. We adapt cage-based deformation for 3DGS by first building a proxy point cloud from the Gaussians and then transferring the point cloud's deformation back to 3DGS, splitting the relevant Gaussians to handle bending. This approach requires no additional training data or architectural changes. We also developed an algorithm that automatically constructs cages for 3DGS deformation.

Limitations Currently, our algorithm simply copies the spherical harmonics parameters for viewpoint-dependent color, without accounting for the effect of rotation. Additionally, compared to cage-based deformation, point-based deformation is better suited for creating smaller deformations, such as facial expressions. Extending 3DGS to capture and edit facial microexpressions is part of our future work.

References

[1] B. Kerbl, G. Kopanas, T. Leimkühler, and G. Drettakis, "3d gaussian splatting for real-time radiance field rendering," *ACM Transactions on Graphics*, vol. 42, no. 4, July 2023. [Online]. Available: https://repo-sam.inria.fr/fungraph/3d-gaussian-splatting/
[2] T. Xu and T. Harada, "Deforming radiance fields with cages," in *ECCV*, 2022.
[3] Y. Peng, Y. Yan, S. Liu, Y. Cheng, S. Guan, B. Pan, G. Zhai, and X. Yang, "Cagenerf: Cage-based neural radiance fields for genrenlized 3d deformation and animation," in *Thirty-Sixth Conference on Neural Information Processing Systems*, 2022.
[4] C. Jambon, B. Kerbl, G. Kopanas, S. Diolatzis, T. Leimkühler, and G. Drettakis, "Nerfshop: Interactive editing of neural radiance fields"," *Proceedings of the ACM on Computer Graphics and Interactive Techniques*, vol. 6, no. 1, May 2023. [Online]. Available: https://repo-sam.inria.fr/fungraph/nerfshop/
[5] J. Waczyńska, P. Borycki, S. Tadeja, J. Tabor, and P. Spurek, "Games: Mesh-based adapting and modification of gaussian splatting," 2024.
[6] A. Guédon and V. Lepetit, "Gaussian frosting: Editable complex radiance fields with real-time rendering," *arXiv preprint arXiv:2403.14554*, 2024.
[7] Y.-H. Huang, Y.-T. Sun, Z. Yang, X. Lyu, Y.-P. Cao, and X. Qi, "Sc-gs: Sparse-controlled gaussian splatting for editable dynamic scenes," *arXiv preprint arXiv:2312.14937*, 2023.
[8] Y. Jiang, C. Yu, T. Xie, X. Li, Y. Feng, H. Wang, M. Li, H. Lau, F. Gao, Y. Yang, and C. Jiang, "Vr-gs: A physical dynamics-aware interactive gaussian splatting system in virtual reality," *arXiv preprint arXiv:2401.16663*, 2024.
[9] B. Huang, Z. Yu, A. Chen, A. Geiger, and S. Gao, "2d gaussian splatting for geometrically accurate radiance fields," in *SIGGRAPH 2024 Conference Papers*. Association for Computing Machinery, 2024.
[10] Y. Chen, Z. Chen, C. Zhang, F. Wang, X. Yang, Y. Wang, Z. Cai, L. Yang, H. Liu, and G. Lin, "Gaussianeditor: Swift and controllable 3d editing with gaussian splatting," 2023.
[11] Y. Wang, X. Yi, Z. Wu, N. Zhao, L. Chen, and H. Zhang, "View-consistent 3d editing with gaussian splatting," *ArXiv*, vol. abs/2403.11868, 2024.
[12] J. Wu, J. Bian, X. Li, G. Wang, I. D. Reid, P. Torr, and V. A. Prisacariu, "Gaussctrl: Multi-view consistent text-driven 3d gaussian splatting editing," *ArXiv*, vol. abs/2403.08733, 2024.
[13] A. Guédon and V. Lepetit, "Sugar: Surface-aligned gaussian splatting for efficient 3d mesh reconstruction and high-quality mesh rendering," *arXiv preprint arXiv:2311.12775*, 2023.
[14] L. Gao, J. Yang, B.-T. Zhang, J. Sun, Y.-J. Yuan, H. Fu, and Y.-K. Lai, "Mesh-based gaussian splatting for real-time large-scale deformation," *ArXiv*, vol. abs/2402.04796, 2024.
[15] X. Gao, X. Li, Y. Zhuang, Q. Zhang, W. Hu, C. Zhang, Y. Yao, Y. Shan, and L. Quan, "Mani-gs: Gaussian splatting manipulation with triangular mesh," *arXiv preprint arXiv:2405.17811*, 2024.
[16] P. Wang, L. Liu, Y. Liu, C. Theobalt, T. Komura, and W. Wang, "Neus: Learning neural implicit surfaces by volume rendering for multi-view reconstruction," *NeurIPS*, 2021.
[17] T. Xie, Z. Zong, Y. Qiu, X. Li, Y. Feng, Y. Yang, and C. Jiang, "Physgaussian: Physics-integrated 3d gaussians for generative dynamics," *arXiv preprint arXiv:2311.12198*, 2023.
[18] C. Jiang, C. Schroeder, J. Teran, A. Stomakhin, and A. Selle, "The material point method for simulating continuum materials," in *ACM SIGGRAPH 2016 Courses*, ser. SIGGRAPH '16. New York, NY, USA: Association for Computing Machinery, 2016. [Online]. Available: https://doi.org/10.1145/2897826.2927348
[19] Y. Feng, X. Feng, Y. Shang, Y. Jiang, C. Yu, Z. Zong, T. Shao, H. Wu, K. Zhou, C. Jiang, and Y. Yang, "Gaussian splashing: Dynamic fluid synthesis with gaussian splatting," 2024.
[20] M. Macklin, M. Müller, and N. Chentanez, "Xpbd: position-based simulation of compliant constrained dynamics," *Proceedings of the 9th International Conference on Motion in Games*, 2016.
[21] W. Zielonka, T. Bagautdinov, S. Saito, M. Zollhöfer, J. Thies, and J. Romero, "Drivable 3d gaussian avatars," 2023.
[22] X. Tong, T. Shao, Y. Weng, Y. Yang, and K. Zhou, " As-Rigid-As-Possible Deformation of Gaussian Radiance Fields ," *IEEE Transactions on Visualization & Computer Graphics*, no. 01, pp. 1–13, Mar. 5555. [Online]. Available: https://doi.ieeecomputersociety.org/10.1109/TVCG.2025.3555404
[23] M. S. Floater, "Mean value coordinates," *Comput. Aided Geom. Des.*, vol. 20, 2003.
[24] T. Ju, S. Schaefer, and J. D. Warren, "Mean value coordinates for closed triangular meshes," *ACM SIGGRAPH 2005 Papers*, 2005.
[25] T. DeRose and M. Meyer, "Harmonic coordinates," 2006.

[26] P. Joshi, M. Meyer, T. DeRose, B. Green, and T. Sanocki, "Harmonic coordinates for character articulation," *ACM Trans. Graph.*, vol. 26, no. 3, p. 71–es, jul 2007. [Online]. Available: https://doi.org/10.1145/1276377.1276466
[27] Y. Lipman, D. Levin, and D. Cohen-Or, "Green coordinates," *ACM SIGGRAPH 2008 papers*, 2008.
[28] S. Li and Y. Pan, "Interactive geometry editing of neural radiance fields," *ArXiv*, vol. abs/2303.11537, 2023.
[29] S. J. Garbin, M. Kowalski, V. Estellers, S. Szymanowicz, S. Rezaeifar, J. Shen, M. A. Johnson, and J. Valentin, "Voltemorph: Real-time, controllable and generalizable animation of volumetric representations," *Computer Graphics Forum*, vol. 43, no. 6, p. e15117, 2024. [Online]. Available: https://onlinelibrary.wiley.com/doi/abs/10.1111/cgf.15117
[30] M. Garland and P. S. Heckbert, "Surface simplification using quadric error metrics," *Proceedings of the 24th annual conference on Computer graphics and interactive techniques*, 1997. [Online]. Available: https://api.semanticscholar.org/CorpusID:621181
[31] C. Xian, H. Lin, and S. Gao, "Automatic generation of coarse bounding cages from dense meshes," *2009 IEEE International Conference on Shape Modeling and Applications*, pp. 21–27, 2009.
[32] S. Calderon and T. Boubekeur, "Bounding proxies for shape approximation," *ACM Transactions on Graphics (Proc. SIGGRAPH 2017)*, vol. 36, no. 5, july 2017.
[33] T. Ju, S. Schaefer, and J. Warren, "Mean value coordinates for closed triangular meshes," in *ACM Siggraph 2005 Papers*, 2005, pp. 561–566.
[34] R. A. Newcombe, S. Izadi, O. Hilliges, D. Molyneaux, D. Kim, A. J. Davison, P. Kohli, J. Shotton, S. Hodges, and A. W. Fitzgibbon, "Kinectfusion: Real-time dense surface mapping and tracking," *2011 10th IEEE International Symposium on Mixed and Augmented Reality*, pp. 127–136, 2011. [Online]. Available: https://api.semanticscholar.org/CorpusID:11830123
[35] Y. Seo, Y. S. Choi, H. S. Son, and Y. Uh, "Flod: Integrating flexible level of detail into 3d gaussian splatting for customizable rendering," 2024. [Online]. Available: https://arxiv.org/abs/2408.12894
[36] Q.-Y. Zhou, J. Park, and V. Koltun, "Open3D: A modern library for 3D data processing," *arXiv:1801.09847*, 2018.
[37] B. Mildenhall, P. P. Srinivasan, M. Tancik, J. T. Barron, R. Ramamoorthi, and R. Ng, "Nerf: Representing scenes as neural radiance fields for view synthesis," in *ECCV*, 2020.
[38] J. T. Barron, B. Mildenhall, D. Verbin, P. P. Srinivasan, and P. Hedman, "Mip-nerf 360: Unbounded anti-aliased neural radiance fields," *CVPR*, 2022.
[39] A. Pumarola, E. Corona, G. Pons-Moll, and F. Moreno-Noguer, "D-nerf: Neural radiance fields for dynamic scenes," *arXiv preprint arXiv:2011.13961*, 2020.
[40] L. Liu, J. Gu, K. Z. Lin, T.-S. Chua, and C. Theobalt, "Neural sparse voxel fields," *NeurIPS*, 2020.
[41] Blender Online Community, *Blender - a 3D modelling and rendering package*, Blender Foundation, Blender Institute, Amsterdam, 2025. [Online]. Available: http://www.blender.org
[42] I. Adobe. (2024) Mixamo: Animate 3d characters for games, film, and more. https://www.mixamo.com.
[43] V. Rong, J. Chen, S. Bahmani, K. N. Kutulakos, and D. B. Lindell, "Gstex: Per-primitive texturing of 2d gaussian splatting for decoupled appearance and geometry modeling," *arXiv preprint arXiv:2409.12954*, 2024.
[44] A. Haque, M. Tancik, A. Efros, A. Holynski, and A. Kanazawa, "Instruct-nerf2nerf: Editing 3d scenes with instructions," in *Proceedings of the IEEE/CVF International Conference on Computer Vision*, 2023.

VII. Biography Section

Jiajun Huang Jiajun Huang is a Ph.D student at the National Centre for Computer Animation (NCCA) of Bournemouth University. He obtained his bachelor's degree from South China Normal University. His research interest covers neural scene representation understanding and editing. Currently, he is conducting research on 3D Gaussian Splatting understanding and animation.

Shuolin Xu Shuolin Xu is a Ph.D student at the National Centre for Computer Animation (NCCA) of Bournemouth University. He obtained his bachelor's degree from Zhengzhou University and his master's degree from Bournemouth University. Currently, he is conducting research on generative models, particularly in the areas of video generation and motion generation.

Hongchuan Yu Hongchuan Yu is a Principal Academic of computer graphics in National Centre for Computer Animation, Bournemouth University, UK. He has published around 110 academic articles in reputable journals and conferences, and regularly served as PC members/referees for international journals and conferences. He is a Member of IEEE (MIEEE) and a fellow of High Education of Academy United Kingdom (FHEA). His research interests include Geometry, GenAI, Graphics, Image, and Video processing.

Tong-Yee Lee Tong-Yee Lee (Senior Member, IEEE) received the Ph.D. degree in computer engineering from Washington State University, Pullman, in 1995. He is currently a chair professor with the Department of Computer Science and Information Engineering, National Cheng-Kung University (NCKU), Tainan, Taiwan. He leads the Computer Graphics Laboratory, NCKU (http://graphics.csie.ncku.edu.tw). His current research interests include computer graphics, nonphotorealistic rendering, medical visualization, virtual reality, and media resizing. He is a Senior Member of the IEEE and a Member of the ACM. He is an Associate Editor of the IEEE Transactions on Visualization and Computer Graphics.

Appendix A
Pseudo-code of Deformation Algorithm

Algorithm 2 GSDeformer Deformation Algorithm

```
Require: 3DGS scene $S_s$, Source Cage $C_s$, Target Cage $C_d$,
         split threshold angle $t$.
Ensure: Deformed 3DGS scene $S_d$
  ret = Empty3DGS()
  for Gaussian $i$ in $GS$ do
      ▷ convert Gaussian to points-represented ellipsoids ◁
      $AP_s$ = point set of $i$ using Equation (3)
      ▷ deform points using cage-based deformation ◁
      $AP_{mvc}$ = EulerToMVC($AP_s$, $C_s$)
      $AP_d$ = MVCToEuler($AP_{mvc}$, $C_d$)
      ▷ perform splitting ◁
      $AP_{ss}$ = $[AP_s]$
      $AP_{ds}$ = $[AP_d]$
      $AP_{ss}$, $AP_{ds}$ = Split($i$, $AP_{ss}$, $AP_{ds}$, $t$)
      ▷ transform Gaussians ◁
      for pre/post transform pair $s_i$, $d_i$ in $AP_{ss}$ and $AP_{ds}$ do
          $\mathbf{T}$ = transform from $s_i$ to $d_i$ using Equation (5)
          $\mathbf{t}$ = $\mathbf{c}$ in $d_i$ - $\mathbf{c}$ in $s_i$
          $i'$ = transform $i$ using Equation (6) and (7)
          append $i'$ to ret
  return ret
```

Algorithm 3 Split Function

```
Require: Gaussian $i$, source points $AP_s$, deformed points
         $AP_d$, split threshold angle $t$.
Ensure: split source points $AP_s$ and deformed points $AP_d$
  for axis $a$ in $\{x, y, z\}$ do
      for deformed ellipsoid $d_i$ in $AP_d$ do
          $c$ = $d_i$'s center
          $l, r$ = endpoints of $d_i$'s $a$ axis
          $\alpha$ = angle formed by $l$-$c$-$r$
          if $\alpha < t$ then
              ▷ Compute split ellipsoid 1 ◁
              $d_l$ = copy of $d_i$
              center of $d_l$ = mean($c$, $l$)
              shift rest of $d_l$ points from $c$ to new center
              make $c$-$l$ $d_l$'s new $a$ axis
              ▷ Compute split ellipsoid 2 ◁
              $d_r$ = copy of $d_i$
              center of $d_r$ = mean($c$, $r$)
              shift rest of $d_r$ points from $c$ to new center
              make $c$-$r$ $d_r$'s new $a$ axis
              ▷ update ellipsoid sets ◁
              replace $d_i$ in $AP_d$ using two ellipsoids $d_l$, $d_r$
              duplicate $d_i$'s source ellipsoid in $AP_s$
  return $AP_s$, $AP_d$
```

Our deformation algorithm is presented in Algorithm 2. The split function is presented in Algorithm 3 . Additionally, it employs EulerToMVC() and MVCToEuler() from cage-based deformation to convert between Euclidean and cage-based coordinates for deformation.

To achieve real-time performance, we perform extensive caching in our implementation. Note that AP_{mvc} and part of T in Algorithm 2 can be precomputed. We also present a simplified implementation of the splitting process that directly operates on the deformed points-represented ellipsoids.

Appendix B
Details of Cage-building Baseline

Inspired by the 3DGS marching cube method proposed by SuGaR [13], our marching cube baseline creates a cage by first converting 3DGS into a binary occupancy voxel grid through opacity thresholding. The process then applies marching cubes to create meshes and simplify them through edge collapse, as proposed by NeRFShop [4].

We transform 3DGS into a binary voxel grid by thresholding each voxel's opacity. A voxel becomes one if its opacity exceeds the threshold and zero otherwise. We calculate voxel opacity $d(\mathbf{v})$ by summing contributions from the K-nearest 3D Gaussians from the voxel center:

$$d(\mathbf{v}) = \sum_g \alpha_g \exp\left(-\frac{1}{2}(\mathbf{v}-\mu_g)^\mathsf{T}\mathbf{\Sigma}_g^{-1}(\mathbf{v}-\mu_g)\right) \quad (12)$$

For each Gaussian g near voxel center $\mathbf{v}$, we use its opacity α_g, mean μ_g, and covariance $\mathbf{\Sigma}_g$. We use a threshold of 1e-6 and K=16 nearest Gaussians.

With the occupancy voxel grid, we mesh it using marching cubes and simplify it using edge collapse to create the final cage.

This cage-building method is later extended to work with 2DGS [9] by converting 2DGS to 3DGS: For every flat ellipse in 2DGS, we compute its third axis as the cross product of the first two axes and set its length to 1e-5, converting 2D ellipses into 3D ellipsoids.